# Green and Facile Fabrication of MWNTs@Sb₂S₃@PPy Coaxial Nanocables for High-Performance Na-Ion Batteries

Sai Wang, Shuang Yuan, Yan-Bin Yin, Yun-Hai Zhu, Xin-Bo Zhang, and Jun-Min Yan*

Renewable intermittent energies such as solar and wind power stimulate energy storage market for low-cost batteries that can store electricity in large scale. Meanwhile battery research has been stimulated towards high energy and high voltage by the development of numerous applications ranging from cell phones, laptops, electric and hybrid energy vehicles.[1,2] During the past two decades, Li-ion batteries (LIBs) have attracted worldwide attention among the various available energy-storage technologies, but when we consider the insufficiency and unevenness of lithium resources in the Earth's crust, Na-ion batteries (NIBs) would be a better choice for the next-generation energy storage system (ESS). NIBs show the same "rocking chair" principle as LIBs, so the utilization of Na instead of Li can mitigate the short supply of lithium sources in an economic way due to the widespread sodium sources and the low price.[3–5] Compared with carbon-based anode materials that exhibit limited capacities,[6–8] metallic and intermetallic materials show a much higher specific capacity via conversion or alloy mechanisms.[3–5,9–13] Chen and co-workers reported an aerosol spray pyrolysis method to prepare ultra-small Sn nanoparticles embedded in carbon with a capacity of 415 mAh g⁻¹ at 1000 mA g⁻¹ for 500 cycles.[9] Sn₄₊ₓP₃@amorphous Sn-P composites reported by Chou et al. delivered a stable capacity of 465 mAh g⁻¹ at 100 mA g⁻¹ over 100 cycles.[10] Zhao and Manthiram obtained Bi–Sb alloy through high-energy mechanical milling and the desodiation capacity of the alloy was 375 mAh g⁻¹ accompanied with a capacity retention of 78% at the 50th cycle.[11] Bao and co-workers synthesized SbOₓ@RGO composite through a wet-milling method and a reversible capacity of 352 mA h g⁻¹ was obtained even at 5 A g⁻¹.[12]

The relatively higher theoretical capacity of Sb₂S₃ made it especially promising among metallic and intermetallic materials.[14–16] Both conversion and alloy mechanisms are involved when Sb₂S₃ is utilized as an anode material for NIBs, one mole of Sb₂S₃ can accommodate twelve moles of electrons and Na⁺ ions. The reaction process could be described as:

$$Sb_2S_3 + 6Na^+ + 6e^- \rightleftharpoons 2Sb + 3Na_2S \qquad (1)$$

$$2Sb + 6Na^+ + 6e^- \rightleftharpoons 2Na_3Sb \qquad (2)$$
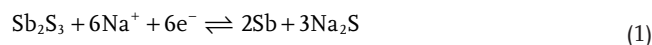
The theoretical capacity for the conversion reaction (Equation (1)) is 473 mAh g⁻¹ and for the whole reaction (Equation (1) + Equation (2)) it is 946 mAh g⁻¹. Although there have been several reports on the Sb₂S₃⁻ and Sb₂S₃⁻-based composites for NIBs, the use of toxic chemical reagents or high energy mechanical instrument was involved in some of the previous works, which might not be suitable for extensive production.[15–20] Therefore, a new method of synthesizing Sb₂S₃⁻ or Sb₂S₃⁻ based composites by an environmental and convenient method with high yield is significant for the commercial process of Sb₂S₃ for NIBs.

Combining nanostructured active materials with electronically conductive matrix has been considered as basic strategy for the design of electrodes for ion batteries.[21–25] Carbon nanotubes (CNTs) are highly conductive and possess good mechanical property, which make them a good choice for enhancing electrochemical properties of the poor conductive active materials. Recently, some novel methods were utilized on the synthesis of CNTs-based materials for ion batteries, red phosphorus-SWCNTs composite as anode material for NIBs was reported by using a facile vaporization-condensation method.[26] Schüth and co-workers fabricated mesoporous Co₃O₄@CNT arrays as anode material for LIBs through a controllable nanocasting process.[27] With the help of electrostatic spray deposition technique, MoS₂–graphene–CNT composites were prepared as anode for LIBs.[28] Besides that, the environmental stability, facile synthesis, high conductivity, and thermal stability make polypyrrole (PPy) a promoting one among the conducting polymers which leading to frequent researches on PPy for improving the electrochemical properties of ion batteries.[29,30]

In this work, a coaxial nanostructure composed of PPy-coated amorphous Sb₂S₃ grafted on multiwalled carbon nanotubes (MWNTs) backbones is reported. The structure is obtained by bottom-up heterogeneous nucleation of amorphous Sb₂S₃ colloids on MWNTs through a solution-based route and subsequent surface-coating by a PPy layer through oxidative polymerization of pyrrole. The MWNTs@Sb₂S₃@PPy nanocables deliver a considerable discharge capacity of 596 mAh g⁻¹ at 100 mA g⁻¹ with a capacity retention of 84% over 80 cycles. The reported green synthesis process of MWNTs@Sb₂S₃@PPy is simple and gives a high yield without the assist of any lethal or volatile toxic chemical substances, the requirement for high

S. Wang, Dr. S. Yuan, Y.-B. Yin, Y.-H. Zhu,
Prof. J.-M. Yan
School of Materials Science and Engineering
Jilin University
Changchun 130012, P. R. China
E-mail: junminyan@jlu.edu.cn
S. Wang, Dr. S. Yuan, Y.-B. Yin, Y.-H. Zhu,
Prof. X.-B. Zhang
State Key Laboratory of Rare Earth Resource Utilization
Changchun Institute of Applied Chemistry
Chinese Academy of Sciences
Changchun 130022, P. R. China

COMMUNICATION
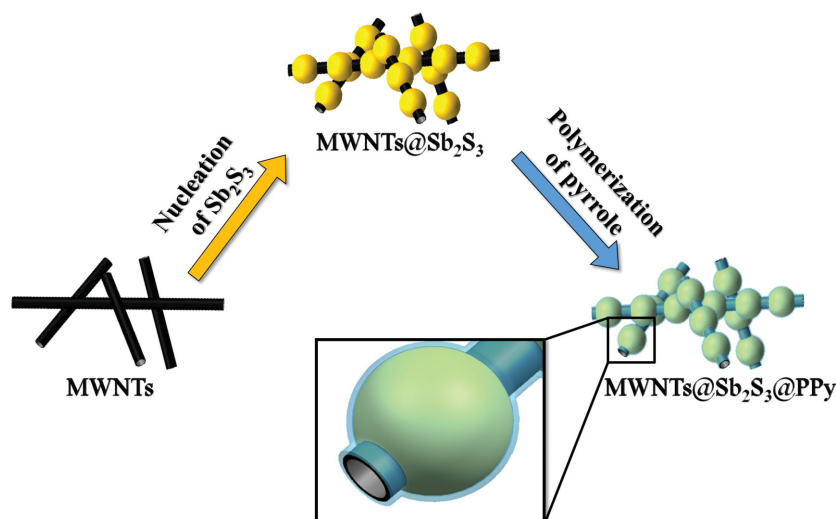
Scheme 1. Schematic illustration of the two-step wet-chemical synthesis method of MWNTs@Sb$_2$S$_3$@PPy.

temperature and special equipment is also avoided, thus this facile synthesis of MWNTs@Sb$_2$S$_3$@PPy might be accessible to an industrial scale.

Scheme 1 demonstrates the synthetic procedure of the MWNTs@Sb$_2$S$_3$@PPy. Generally, amorphous Sb$_2$S$_3$ colloids can be gradually formed in the progress of dropping the CH$_3$CSNH$_2$ ethanol solution into the SbCl$_3$ ethanol solution at 50 °C. When the SbCl$_3$ solution contains a certain amount of MWNTs, Sb$_2$S$_3$ colloids prefer to form on the surface of MWNTs through the heterogeneous nucleation mechanism. Next the pyrrole monomer can be readily polymerized at room temperature on the surface of MWNTs@Sb$_2$S$_3$ with C$_{12}$H$_{25}$SO$_4$Na and (NH$_4$)$_2$S$_2$O$_8$ which acts as directing agent and oxidizer, respectively. In the coaxial nanocables not only the charge transfer can be facilitated by the three-dimensional (3D) network of MWNTs but also the volume expansion, dissolution and aggregation of Sb$_2$S$_3$ can be alleviated by the PPy layer. For convenience, in the next paragraphs "MS" and "MSP" are set as logograms for "MWNTs@Sb$_2$S$_3$" and "MWNTs@Sb$_2$S$_3$@PPy", respectively.

Figure 1a shows the X-ray diffraction (XRD) patterns of the bare MWNTs, the as synthesized MS and MSP. The two peaks at 26° and 43° of MWNTs are respectively indexed to the (002) and (101) reflections of hexagonal graphite. But there are no obvious crystalline Sb$_2$S$_3$ phases can be identified for both of the as-synthesized MS and MSP. This indicates the structure of the Sb$_2$S$_3$ in the two composites is amorphous. As can be seen from the insets of Figure 1a, the samples color changes obviously during the two-step synthetic procedure which is in line with Scheme 1, namely the optical color of the bare MWNTs turns from black to atrovirens after the nucleation of Sb$_2$S$_3$ and the optical color of MS turns from atrovirens to black blue after the polymerization of pyrrole. X-ray photoelectron spectroscopy (XPS) measurements were further performed for confirmation of the existence of Sb$_2$S$_3$ in MS. Figure 1b exhibits the O 1s peaks of the MWNTs, the two main peaks in the range of 535 to 530 eV can be indexed to the presence of some carboxylic and hydroxyl functions such as C–O–C, C–O–OH, C–OH,

C=O, O–C=O onto the MWNTs surface.[31,32] In addition to the O1s peaks, Figure 1c shows the presence of two extra peaks for Sb 3d$_{3/2}$ and Sb 3d$_{5/2}$ at 538.25 eV and 528.75 eV, respectively.[33] In Figure 1d the S 2p spectrum of MS shows two peaks at 162 eV for S 2p$_{1/2}$ and 160.8 eV for S 2p$_{3/2}$, which is a powerful evidence of sulfide formation on the MWNTs.[34] In order to accurately confirm the existence of Sb$_2$S$_3$ in MS, energy-dispersive X-ray spectroscopy (EDX) was carried on as shown in Figure 1e. Ignore Cu, C, and O elements originate from the TEM support film or the MWNTs, the elemental stoichiometry of MS is focused on the two investigated spots and the result indicates the atomic ratio of Sb:S is 8.32:11.57, which is close to the ideal ratio 2:3. All of these spectrometric analyses provide sufficient evidences for the existence of amorphous Sb$_2$S$_3$ in MS.

Scanning electron microscopy (SEM) was performed to observe the morphology change from the bare MWNTs to the MSP. As shown in the Figure S1a,b (Supporting Information), the surface of the bare MWNTs is smooth and their diameters are about 10–15 nm. Obviously, after the Sb$_2$S$_3$ nucleation procedure, Sb$_2$S$_3$ particles with sphere or cylinder shapes are anchoring uniformly on the surfaces of the MWNTs and no aggregation of Sb$_2$S$_3$ is found. The average diameter of MS nanocables is about 40–50 nm (Figure S1c,d, Supporting Information). It is also evident that after the polymerization of pyrrole, PPy also is not tend to agglomerate (grows into micron or submicron particles) (Figure S1e,f, Supporting Information). There seems no obvious difference in morphology between MS and MSP except that the diameters of the former are thinner than the later (50–60 nm). Transmission electron microscope (TEM) was used to further examine the morphology difference between the two samples. The TEM images of MS (**Figure 2**a,b) illustrate that Sb$_2$S$_3$ particles anchor on the MWNTs tightly with a smooth and clean surface. After the polymerization of pyrrole, the surface of the composites (Figure 2c,d) becomes very rough and there is a clear boundary can be observed between Sb$_2$S$_3$ and PPy. The average thickness of the PPy layer is about 5–10 nm. In addition, Selected area electron diffraction (SAED) patterns of MS with faint rings diffraction spots (Figure 2e) also indicate the amorphous structure of Sb$_2$S$_3$ and the elemental mapping images of MS (Figure 2f) confirm the uniform distribution of S and Sb elements around the MWNTs. The N element originated from PPy could be clearly seen and distributed uniformly on MSP as exhibited in Figure S2, Supporting Information, which demonstrated the uniform coating of PPy on MS.

The existence of the PPy layer in MSP was also proved by Fourier transform infrared spectroscopy (FTIR) spectra as shown in **Figure 3**a. Compared with the FTIR spectra of the MWNTs and MS, the corresponding characteristic transmittances of PPy in the spectra of MSP were obviously observed at 1687.4, 1554.7, 1197.7, 1037.3, and 918.5 cm^{-1}, which are similar to those reported for PPy synthesized with different reaction conditions.[35–37] The peak at 1687.4 cm^{-1} is attributed
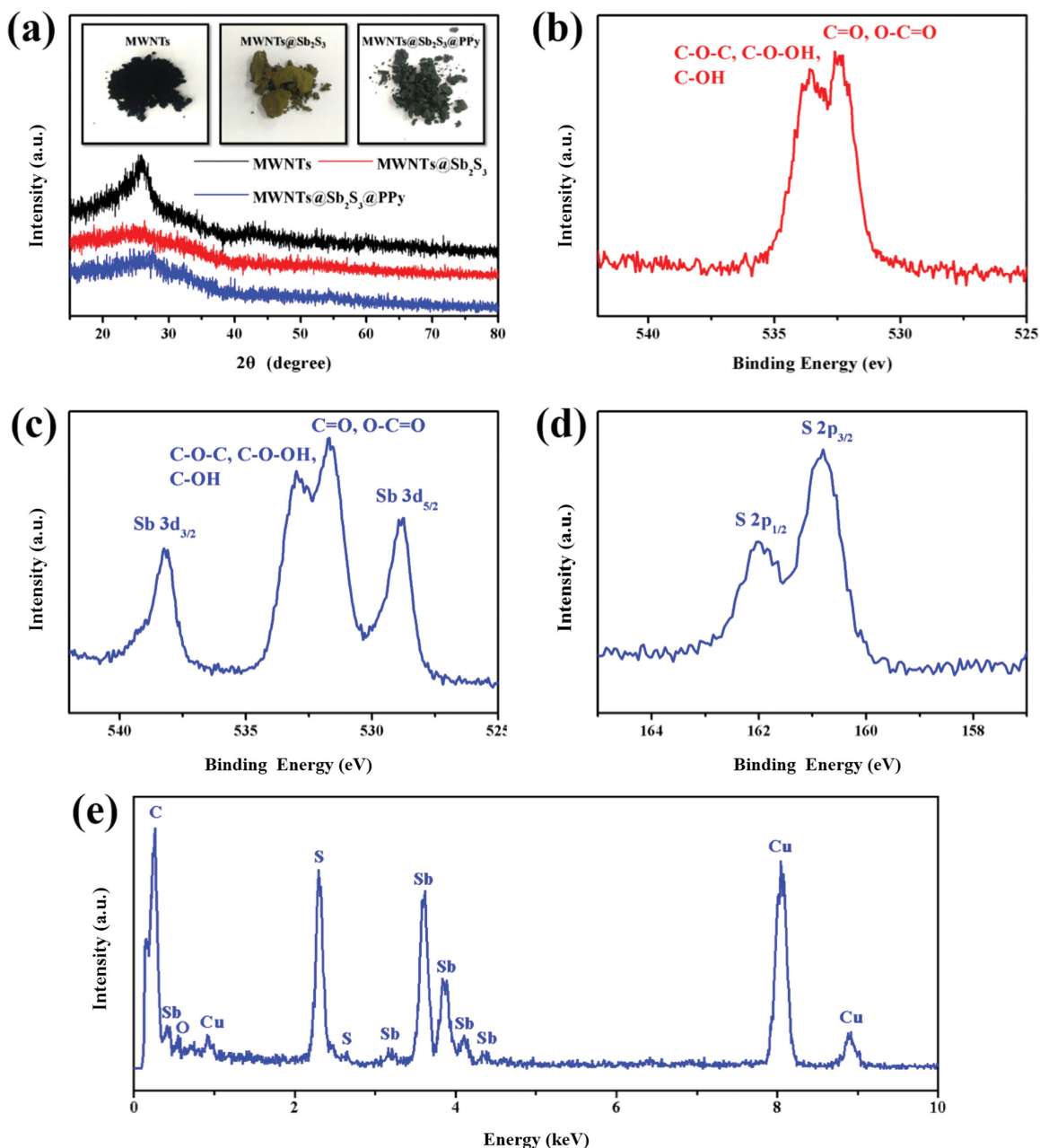
Figure 1. a) XRD patterns of the bare MWNTs, the as synthesized MS and MSP and the insets are the optical images of the three samples. b) XPS spectrum of O 1s of the bare MWNTs. c) XPS spectrum of O 1s and Sb 3d of MS. d) XPS spectrum of S 2p of MS. e) EDX spectroscopy of MS.

to C—N bond and the peak at 1554.7 cm^{-1} corresponds to the C=C stretching. The peak at 1197.7 cm^{-1} corresponds to the breathing vibration of the pyrrole ring. The peaks at 1037.3 cm^{-1} and 918.5 cm^{-1} are attributed to the in-plane and out-of-plane deformation vibrations of C—H band on the pyrrole ring, respectively. In consistent with the TEM results, these results also demonstrate that the PPy layer has uniformly formed on the surface of MS.

Thermogravimetric analysis (TGA) (Figure 3b) was applied to determine the content in each of the two composites. The weight ratio between MWNTs and Sb$_2$S$_3$ in MS is about 24:76 and the weight ratio between MWNTs, Sb$_2$S$_3$ and PPy in MSP

is about 19:59:22. The calculations are based on the fact that the remaining products after heat treatments of MS and MSP from room temperature to 800 °C at a heating rate of 10 °C min^{-1} in a muffle furnace are pure phase Sb$_2$O$_4$ (Figure S3, Supporting Information). The conversion from Sb$_2$S$_3$ to Sb$_2$O$_4$ during high-temperature treatment is in conformity with the literature that previously reported on the TGA analysis of Sb$_2$S$_3$.[38]

Coin cells with metallic Na as counter electrodes were assembled to evaluate the electrochemical properties of MSP and MS. **Figure 4**a shows the cyclic voltammograms (CV) curves of MSP vs. Na$^+$/Na at a scan rate of 0.025 mV s^{-1} between 0 and 2 V. In the first cathodic scan, a sharp peak at 0.8 V is attributed to
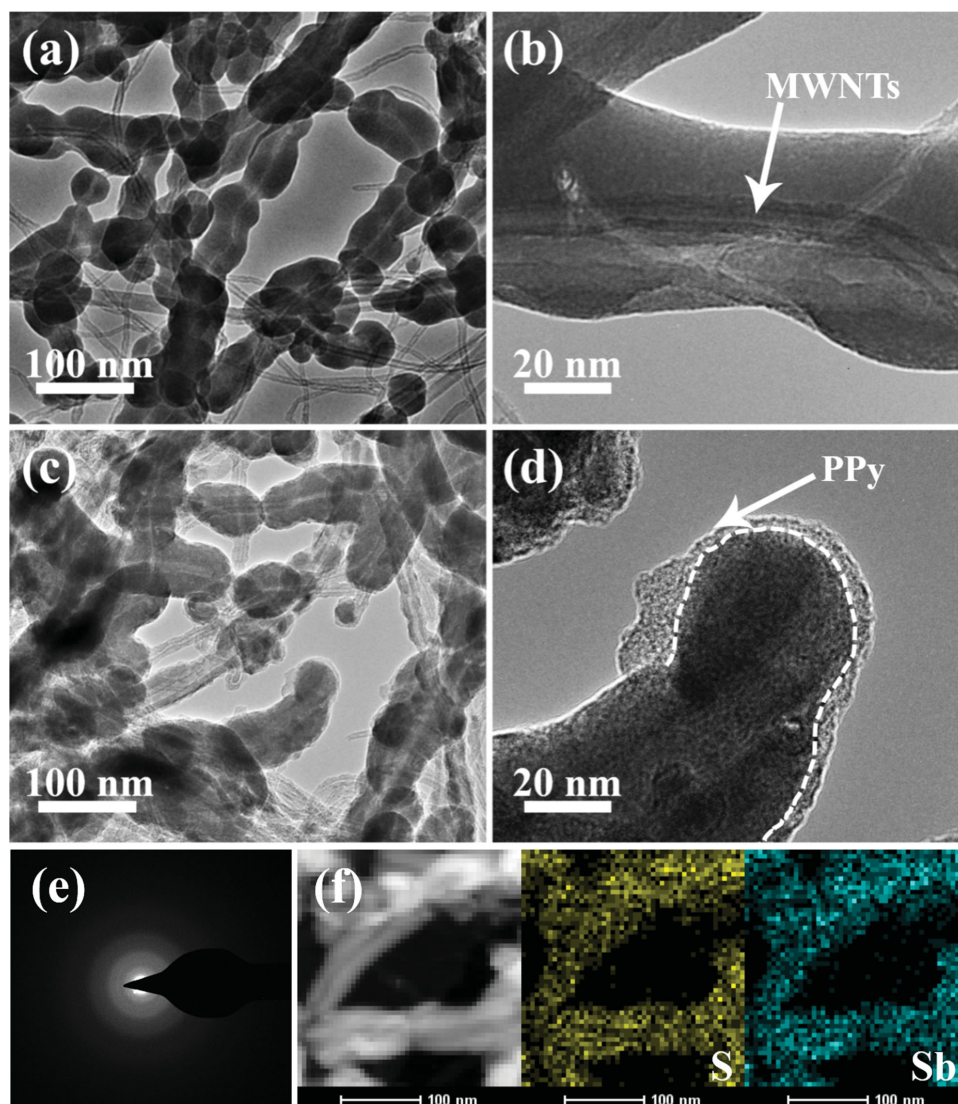
Figure 2. a,b) TEM images of MS. c,d) TEM images of MSP. e) SAED patterns of MS. f) Elemental mapping images of MS.
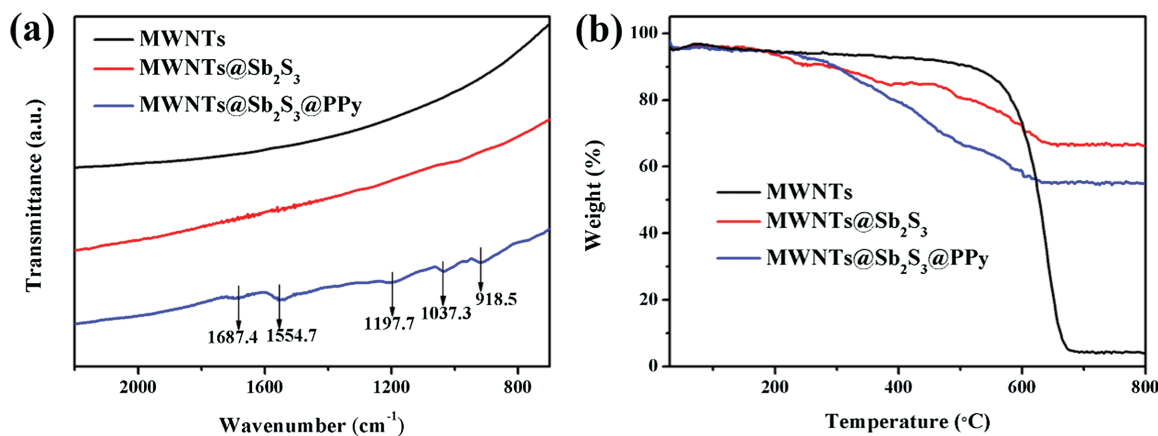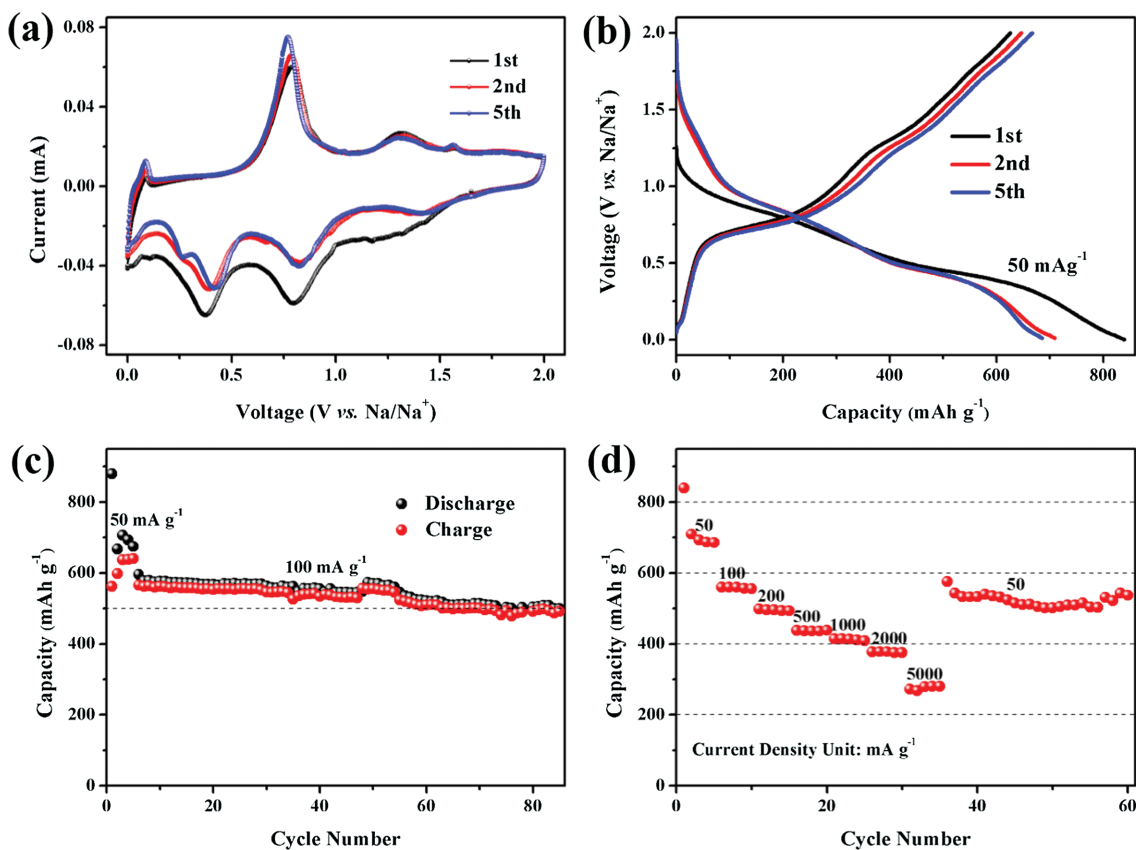

Figure 3. a) FTIR spectra of the MWNTs, MS, and MSP. b) TGA curves of the MWNTs, MS, and MSP.

Figure 4. a) CV curves of MSP. b) Discharge–charge curves of MSP at 50 mA g^{-1}. c) Cycle performance of MSP at 100 mA g^{-1}. d) Rate performance of MSP.

the reaction between Na$^+$ with sulfur atoms (Equation (1)) and some irreversible decomposition of the electrolyte results in forming a solid-electrolyte interface (SEI) film. The second and third peaks at 0.37 and 0 V correspond to Na$^+$ alloying reaction with Sb (Equation (2)) and Na$^+$ insertion into MWNTs, respectively.[15,16,39–41] The reaction between Na$^+$ and the MWNTs is also evidenced by the CV curves of the MWNTs vs. Na$^+$/Na as shown in Figure S4a (Supporting Information). The MWNTs give a relatively high initial discharge capacity of 963 mA g^{-1} (Figure S4b, Supporting Information), which is consistent with the two strong irreversible CV peaks at 1 and 0.5 V that originate from the SEI formation on different active surfaces of the MWNTs.[41] In the first anodic scan, three peaks at 0.09, 0.79, and 1.32 V correspond to Na$^+$ extraction out of MWNTs, Na-Sb dealloying reaction (Equation (2)) and Na$_2$S-Sb conversion reaction (Equation (1)), respectively. In the second and subsequent scans, the cathodic peaks shift to relatively high potentials and the areas between the CV curves become smaller, which is in line with the forming of SEI in the first discharge progress. During the first scan, the absence of the cathodic peak around 0.26 V (emerges from the second scan) corresponds the alloying reaction between Na$^+$ and Sb, which may be covered by the peak originates from the SEI formation on the MWNTs and this phenomenon appears both for MSP and MS. Thus in the succeeding scans the potential pairs at 0.83/1.32 V; 0.26, 0.38/0.79 V; 0/0.09V separately agree well with the conversion–deconversion reactions between Na$^+$ and sulfur atoms

(Equation (1)); the alloying–dealloying reactions between Na$^+$ and Sb (Equation (2)); the insertion-extraction reactions between Na$^+$ and the MWNTs. As shown in Figure S5a (Supporting Information), cyclic voltammetry was also carried out on MS electrode, it can be observed that the CV peaks of MS show almost same locations as compared with the PPy-coated one, indicating the two samples share the same electrochemical reaction mechanism.

The discharge–charge curves of MSP and MS at three different cycles at a current density of 50 mA g^{-1} are shown in Figure 4b and Figure S5b (Supporting Information). It is worth stressing that all of the capacities are calculated based on the mass of the whole active materials rather than only the Sb$_2$S$_3$. The initial discharge curves of the two composite powders are consisted of slight plateaus near 1 and 0.5 V, which are in agreement with the two cathodic peaks observed at 0.8 and 0.37 V. Two weak charge plateaus can be observed at around 0.8 and 1.4 V, corresponding well with the two oxidation peaks at 0.79 and 1.32 V in the CV curves. The initial discharge and charge capacities of MSP are 839 and 626 mAh g^{-1} and the corresponding capacities of MS are 844 and 742 mAh g^{-1}. The initial capacities and the initial Coulombic efficiency of MSP (75%) are lower than that of MS (88%) which should be attributed to the relative extra inactive PPy film (22% weight of MSP) as the PPy particles only give a reversible capacity about 25 mAh g^{-1}. The role of the MWNTs in enhancing the electrochemical properties of MS is obviously seen as the bare Sb$_2$S$_3$ particles only give a lower

initial discharge capacity of 612 mA g^{-1} accompanied with a fairly low Coulombic efficiency (63%) and the discharge capacity fades quickly to 332 mA g^{-1} at 24 cycles (Figure S4b,c, Supporting Information). The electrochemical impedance spectroscopy (EIS) results demonstrate that the charge transfer resistance of the materials decreases from Sb$_2$S$_3$ to MSP, which indicates that both MWNTs and PPy films play roles in guaranteeing the charge transfer of the composites (Figure S4d, Supporting Information).

The cycling performance between 0 and 2 V at a current density of 100 mA g^{-1} of MSP is shown in Figure 4c. After five cycles activation at 50 mA g^{-1}, MSP delivers a considerable discharge capacity of 596 mAh g^{-1} at 100 mA g^{-1}. The 85th (80th at 100 mA g^{-1}) reversible discharge and charge capacities of MSP are 500 and 492 mAh g^{-1}, respectively, the corresponding capacity retention measured after the five activation cycles is 84%. MS delivers relatively high discharge capacities above 650 mAh g^{-1} at 50 mA g^{-1} in the initial cycles, actually, the capacities fade quickly and a considerable discharge capacity of 511 mAh g^{-1} can be obtained after 33 cycles. The capacity of MS fades dramatically at 100 mA g^{-1} with a capacity retention of only 9% after the 80th cycle (Figure S5c, Supporting Information). To gain additional insight, the rate tests of MSP and MS were also measured (Figure 4d and Figure S5d, Supporting Information). MSP shows a remarkable rate performance with reversible discharge capacities 690 mAh g^{-1} at 50 mA g^{-1}, 560 mAh g^{-1} at 100 mA g^{-1}, 495 mAh g^{-1} at 200 mA g^{-1}, 436 mAh g^{-1} at 500 mA g^{-1}, 413 mAh g^{-1} at 1000 mA g^{-1}, 376 mAh g^{-1} at 2000 mA g^{-1} and 280 mAh g^{-1} at a relatively high rate of 5000 mA g^{-1}. As the rate is reset to 50 mA g^{-1}, stable discharge capacities above 500 mAh g^{-1} over 25 cycles can be obtained. When it comes to MS although at some low current densities the composite exhibits higher capacities than MSP, the capacities fade obviously at current densities higher than 200 mA g^{-1} and the composite exhibits a relatively low capacity of 46 mAh g^{-1} at 5000 mA g^{-1}. There is no considerable cycle performance can be obtained as the rate is reset to 50 mA g^{-1} for MS. To directly demonstrate that the unique coaxial nanostructure causes MSP to have a considerable electrochemistry performance, Sb$_2$S$_3$, PPy, and MWNTs with weight ratio 19:59:22 (the same as MSP) were also directly mixed as active materials to make the electrodes, which show a negligible electrochemical performance as shown in Figure S6 (Supporting Information).

Such a unique hybrid structure of MSP manifests improved electrochemical performance should be explained through the following reasons. (i) The highly conductive and flexible MWNTs matrix could provide a 3D electronic network for the electrolyte easily diffusing into the internal electrode area.[26–28,41] (ii) The nanoscale Sb$_2$S$_3$ could provide more active sites for electrochemical reaction, which would be in favour of releasing higher capacity.[3,4] (iii) Except guaranteeing the charge transfer, the outmost ductile PPy layer could also maintain the integrity of the electrode structure through further relieving the volume expansion and acting as a protective layer to alleviate the dissolution of Sb$_2$S$_3$.[29,30] Thus the integration of these advantageous structural features makes MSP demonstrate a considerable electrochemical performance.

In summary, MWNTs@Sb$_2$S$_3$@PPy coaxial nanocables have been obtained by a two-step wet-chemical method through bottom-up heterogeneous nucleation of amorphous Sb$_2$S$_3$ colloids on MWNTs and subsequent surface-coating by PPy layer. A considerable discharge capacity of 596 mAh g^{-1} at 100 mA g^{-1} with capacity retention of 84% over 80 cycles can be obtained as the nanocables are employed as anode material for NIBs. Importantly, the green synthetic procedure of the MWNTs@Sb$_2$S$_3$@PPy is simple and high-yield without the assist of lethal or volatile chemical substances, high temperature or special equipment. All of these indicate its potential in NIBs industrial technologies in the future.

Supporting Information

Supporting Information is available from the Wiley Online Library or from the author.

Acknowledgements

[1] M. Armand, J. M. Tarascon, *Nature* **2008**, *451*, 652.

[2] B. Dunn, H. Kamath, J. M. Tarascon, *Science* **2011**, *334*, 928.

[3] V. Palomares, P. Serras, I. Villaluenga, K. B. Hueso, J. Carretero-González, T. Rojo, *Energy Environ. Sci.* **2012**, *5*, 5884.

[4] H. L. Pan, Y. S. Hu, L. Q. Chen, *Energy Environ. Sci.* **2013**, *6*, 2338.

[5] S.-W. Kim, D.-H. Seo, X. Ma, G. Ceder, S. Kang, *Adv. Energy Mater.* **2012**, *2*, 710.

[6] S. Wenzel, T. Hara, J. Janek, P. Adelhelm, *Energy Environ. Sci.* **2011**, *4*, 3342.

[7] S. Komaba, W. Murata, T. Ishikawa, N. Yabuuchi, T. Ozeki, T. Nakayama, A. Ogata, K. Gotoh, K. Fujiwara, *Adv. Funct. Mater.* **2011**, *21*, 3859.

[8] K. Tang, L. Fu, R. J. White, L. Yu, M.-M. Titirici, M. Antonietti, J. Maier, *Adv. Energy Mater.* **2012**, *2*, 873.

[9] Y. Liu, N. Zhang, L. Jiao, Z. Tao, J. Chen, *Adv. Funct. Mater.* **2015**, *25*, 214.

[10] W. Li, S.-L. Chou, J.-Z. Wang, J. H. Kim, H.-K. Liu, S.-X. Dou, *Adv. Mater.* **2014**, *26*, 4037.

[11] Y. Zhao, A. Manthiram, *Chem. Mater.* **2015**, *27*, 3096.

[12] X. Zhou, X. Liu, Y. Xu, Y. Liu, Z. Dai, J. Bao, *J. Phys. Chem. C* **2014**, *118*, 23527.

[13] L. Hu, X. Zhu, Y. Du, Y. Li, X. Zhou, J. Bao, *Chem. Mater.* **2015**, *27*, 8138.

[14] H. Hou, M. Jing, Z. Huang, Y. Yang, Y. Zhang, J. Chen, Z. Wu, X. Ji, *ACS Appl. Mater. Interfaces* **2015**, *7*, 19362.

[15] D. Y. W. Yu, P. V. Prikhodchenko, C. W. Mason, S. K. Batabya, J. Gun, S. Sladkevich, A. G. Medvedev, O. Lev, *Nat. Commun.* **2013**, *4*, 2922.

[16] Y. Zhu, P. Nie, L. Shen, S. Dong, Q. Sheng, H. Li, H. Luo, X. Zhang, *Nanoscale* **2015**, *7*, 3309.

[17] C.-H. Lee, C.-L. Wang, H.-F. Lin, C.-Y. Chai, M.-Y. Hong, C.-K. Ho, *Toxicol. Ind. Health* **2011**, *27*, 497.

[18] C.-L. Wu, S.-B. Su, J.-L. Chen, H.-J. Lin, H.-R. Guo, *J. Occup. Health* **2008**, *50*, 99.

[19] G. Marino, H. Anastopoulos, A. D. Woolf, *J. Occup. Med.* **1994**, *36*, 637.

498 wileyonlinelibrary.com

© 2016 WILEY-VCH Verlag GmbH & Co. KGaA, Weinheim

Part. Part. Syst. Charact. **2016**, *33*, 493–499

[20] Y. Zhao, A. Manthiram, *Chem. Commun.* **2015**, *51*, 13205.

[21] A. L. M. Reddy, M. M. Shaijumon, S. R. Gowda, P. M. Ajayan, *Nano Lett.* **2008**, *9*, 1002.

[22] H. Gwon, H.-S. Kim, K. U. Lee, D.-H. Seo, Y. C. Park, Y.-S. Lee, B. T. Ahn, K. Kang, *Energy Environ. Sci.* **2011**, *4*, 1277.

[23] Z. Wang, D. Luan, S. Madhavi, Y. Hu, X. W. Lou, *Energy Environ. Sci.* **2012**, *5*, 5252.

[24] J. Song, Z. Yu, M. L. Gordin, S. Hu, R. Yi, D. Tang, T. Walter, M. Regula, D. Choi, X. Li, A. Manivannan, D. Wang, *Nano Lett.* **2014**, *14*, 6329.

[25] S. H. Choi, Y. N. Ko, J.-K. Lee, Y. C. Kang, *Adv. Funct. Mater.* **2015**, *25*, 1780.

[26] Y. Zhu, Y. Wen, X. Fan, T. Gao, F. Han, C. Luo, S.-C. Liou, C. Wang, *ACS Nano* **2015**, *9*, 3254.

[27] D. Gu, W. Li, F. Wang, H. Bongard, B. Spliethoff, W. Schmidt, C. Weidenthaler, Y. Xia, D. Zhao, F. Schüth, *Angew. Chem. Int. Ed.* **2015**, *54*, 7060.

[28] C. Zhu, X. Mu, P. A. van Aken, J. Maier, Y. Yu, *Adv. Energy Mater.* **2015**, *5*, 1401170.

[29] P. Novák, K. Müller, K. S. V. Santhanam, O. Haas, *Chem. Rev.* **1997**, *97*, 207.

[30] W. Tang, L. Liu, Y. Zhu, H. Sun, Y. Wu, K. Zhu, *Energy Environ. Sci.* **2012**, *5*, 6909.

[31] J. A. Kim, D. G. Seong, T. J. Kang, J. R. Youn, *Carbon* **2006**, *44*, 1898.

[32] V. Datsyuk, M. Kalyva, K. Papagelis, J. Parthenios, D. Tasis, A. Siokou, I. Kallitsis, C. Galiotis, *Carbon* **2008**, *46*, 833.

[33] W. Lou, M. Chen, X. Wang, W. Liu, *Chem. Mater.* **2007**, *19*, 872.

[34] P. V. Prikhodchenko, J. Gun, S. Sladkevich, A. A. Mikhaylov, O. Lev, Y. Y. Tay, S. K. Batabyal, D. Y. W. Yu, *Chem. Mater.* **2012**, *24*, 4750.

[35] M. Omastová, M. Trchová, J. Kovářová, J. Stejskal, *Synth. Met.* **2003**, *138*, 447.

[36] S. Ye, L. Fang, Y. Lu, *Phys. Chem. Chem. Phys.* **2009**, *11*, 2480.

[37] M. A. Chougule, S. G. Pawar, P. R. Godse, R. N. Mulik, S. Sen, V. B. Patil, *Soft Nanosci. Lett.* **2009**, *1*, 6.

[38] H. Jang, S. J. Kim, *Wear* **2000**, *239*, 229.

[39] M. He, K. Kravchyk, M. Walter, M. V. Kovalenko, *Nano Lett.* **2014**, *14*, 1255.

[40] A. Darwiche, C. Marino, M. T. Sougrati, B. Fraisse, L. Stievano, L. Monconduit, *J. Am. Chem. Soc.* **2012**, *134*, 20805.

[41] Y. Cao, L. Xiao, M. L. Sushko, W. Wang, B. Schwenzer, J. Xiao, Z. Nie, L. V. Saraf, Z. Yang, J. Liu, *Nano Lett.* **2012**, *12*, 3783.